First International Symposium on Fishing Vessel Energy Efficiency
E-Fishing, Vigo, Spain, May 2010

Experimental analysis of the characteristics of the flow around bottom trawls

Elkhadim Bouhoubeiny[1-2], Grégory Germain[1], Philippe Druault[2]

1 Hydrodynamic & Metocean Service, IFREMER, 150 Quai Gambetta, 62321 Boulogne-sur-Mer, France.
2 University Pierre et Marie Curie-Paris 6, IJLRA, Case 162, 4 Place Jussieu, 75252 Paris cedex 5, France.

***Abstract*—The work presented in this paper is carried out under the HydroPêche project with the aim to develop a tool for an automatic optimisation of trawl in order to minimize the drag of the gear. One of the aspects of this project is the experimental investigation of the turbulent flow around bottom trawls.**

For that purpose, Particle Image Velocimetry measurements in a flume tank are implemented to access to the two-dimensional velocity field around a bottom trawl. Having an important experimental database allows not only the calibration of numerical models aiming at simulating the flow around a fishing net but also the validation of numerical simulation results. Such experimental technique has the advantage in accessing the turbulent flow field and then allows the determination of the main turbulent flow characteristics. Then Proper Orthogonal Decomposition analysis was applied to extract the main coherent structures of the overall physical phenomenon from the measured database. Finally, a spectral analysis of the longitudinal velocity is applied to determine the frequency of the vortex shedding. This analysis show that the Strouhal number is between 0.19-0.3 in this case.

Keywords – Experimental trials ; Particle Image Velocimetry; Bottom Trawl ; Vortex Shedding ; Proper Orthogonal Decomposition

I. INTRODUCTION

Knowing that the trawls are responsible of the largest part of the fuel consumption during fishing operations: most of the fuel consumed during a fishing trip is used to tow the fishing gear, an important work should be done on this area to increase energy efficiency. Indeed, the hydrodynamic behaviour of porous structures used for bottom or pelagic trawls is still poorly understood. The complexity of the flow makes numerical simulations difficult and today no effective model exists.

The work presented here is a part of the HydroPêche* project [1] whose goal is to develop a tool for automatic optimisation of trawl in order to minimize the drag of the gear. For that purpose, different aspects are studied in order: a/ to extend the basis of experimental data on flow characteristics governing the hydrodynamic behaviour of different porous structures, b/ to develop numerical tools to simulate more realistic flow around porous structures taking into account fluid / structure interactions and c/ to develop automatic optimisation tools to design efficient trawls in terms of energy consumption.

This paper deals with the first aspect of this project, *i.e.* the experimental investigation of the turbulent flow around bottom trawls. From a better knowledge of the flow characteristics, the improvement of the structural analysis of a net structure taking into account the effect of the trawl on the inflow condition will be possible. As well known, the flow and thus the drag forces on net structures are strongly dependent with both the geometry (Solidity ratio) and the Reynolds number. If it is evident that for increasing Solidity ratios, flow interaction will become increasingly significant, these perturbations are not well known and easily characterized. So, in order to evaluate these effects and to identify the areas where the drag is generated, we have carried out an experimental work to characterise the flow characteristics around two kinds of structure: a/ a 1/10 scale bottom trawl and b/ a rigid cod-end. The bottom trawl is used in order to determine the evolution of the boundary layer along the structure while the rigid cod-end is used in order to characterise the turbulent flow in this specific region. The flow is characterized from Particle Image Velocimetry (PIV) measurements.

* Project supported by the European Fisheries Fund and the French Ministry of Agriculture and Fisheries

In this paper we present both the experimental results and the tools used for the post processing (a Proper Orthogonal Decomposition method) and the spectral analysis of the experimental data.

II. EXPERIMENTAL DEVICE

Experimental campaigns carried out for this project are performed in the Ifremer (French Research Institute for Exploitation of the Sea) wave-current circulation flume tank. This flume tank (see Figure 1) is a 18 m long by 4 m wide and 2 m deep recirculating channel. A side observation window of 8 m x 2 m placed on one side of the tank allows users to observe the behaviour of the models during trials and to carry out video sequences. The bottom of the flume is a conveyor belt which can be synchronized with the water speed in order to simulate devices in contact with the bottom, like bottom trawls. The flow turbulence can be adjusted between 5 to 28 % and the flow velocity range is 0.1 to 2.2 m/s.

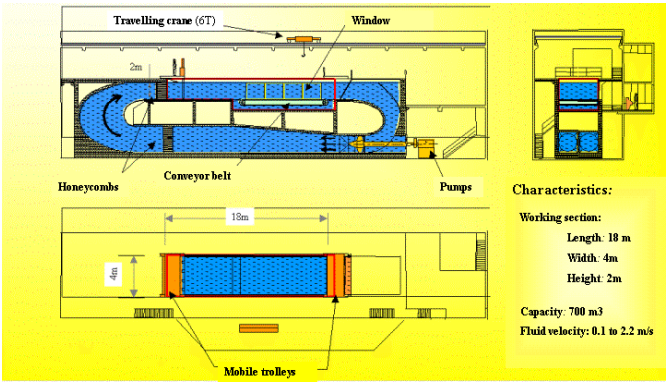

Figure 1. Ifremer free surface hydrodynamic water tunnel.

A. MEASUREMENT SYSTEM

In this work, the velocity fields are obtained using PIV technique measurement. The PIV system, shown in Figure 2, is composed of a double pulsed laser type two-chamber Gemini PIV Nid-Yag 2 x 120 mJ at 15 Hz, and a CCD camera Hi sense. The method that records the measurement of the existing velocities around fishing gear in the flume tank offers two main advantages: (1) it is non-intrusive and (2) it offers the possibility of mapping the velocities on one or more planes, in real time, and under unsteady conditions. This technique is based on illuminating the seeding particles and storing the resulting camera images to analyze displacements of particles between two successive images. The velocities are obtained by dividing the distance by the elapse time of laser pulses.

In the flume tank two cameras are available with two different objectives (focal lens). The first camera has a 4 Hz frequency, with a 1280 x 1024 pixels^2 resolution. The second one has a 15 Hz frequency, with a 1600 x 1200 pixels^2 resolution. The measurement plane corresponding to the focal lens length of 60 mm is 810.7 x 648.5mm^2, while the measurement plane corresponding to the focal lens length of 20 mm is 387.91 x 290.843 mm^2. The image processing is done with the Flow Map 1500 software from Dantec dynamics. It is based on image intercorrelation on regions of 32 x 32 pixels^2, with a covering rate of 25%. The vector field was evaluated by a predefined velocity magnitude and the invalid one was replaced by the moving average method. Instantaneous velocity fields were obtained and generally, a series of instantaneous measurements were statistically average to get the mean velocity field. The instantaneous and mean velocity fields and turbulence quantities are of great practical interests.

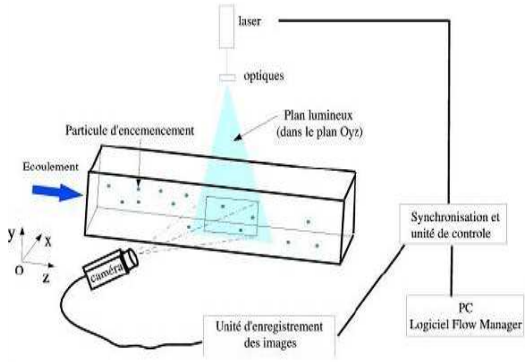

Figure 2. PIV system principle.

B. DESCRIPTION OF PIV CAMPAIGNS

Three experimental campaigns have been successively performed. In each campaign, PIV system is implemented to determine the instantaneous velocity field. More precisely, the longitudinal u and transverse v velocity components are accessed along the y and z directions respectively.

The two fist campaigns deal with the fishing gear using a rigid cod-end (see figure 3 and [2]). This structure is axi-symmetric and the catch inside the cod-end is limited by two spherical caps, so its shape is known. The 1/6 scaled model is 1 m long, made of PA twine of 1200 m/kg, with diamond-shaped meshes of 30 mm lens. During the third campaign the turbulent flow around a bottom trawl has been studied.

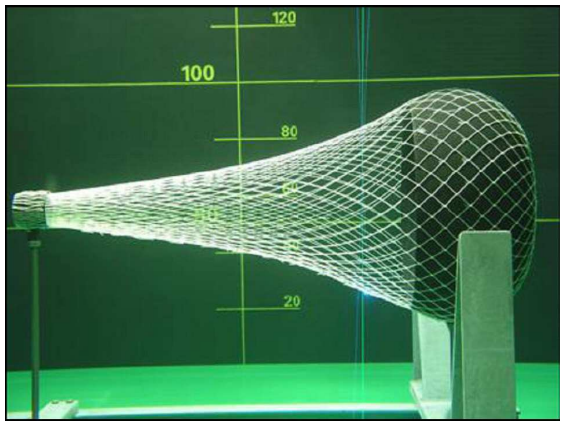

Figure 3. Rigid cod end in the flume tank.

1. First measurement campaign

In this campaign, the focal lens length of the camera is 60 mm, the size of the image is 810.7 x 648.5 mm^2, or 1280 x 1024 $pixels^2$. The laser is placed behind the catch of the rigid cod-end and the camera is outside. The time between two pulses laser adjusted to 0.25 s, and two 190 successive velocity fields are measured for a total time of 95 s. The distance between tow points of mesh is 15.2 mm on the Oy axis and 15.2 mm on the Oz axis. The measurement is carried out in two planes shown in Figure 4.

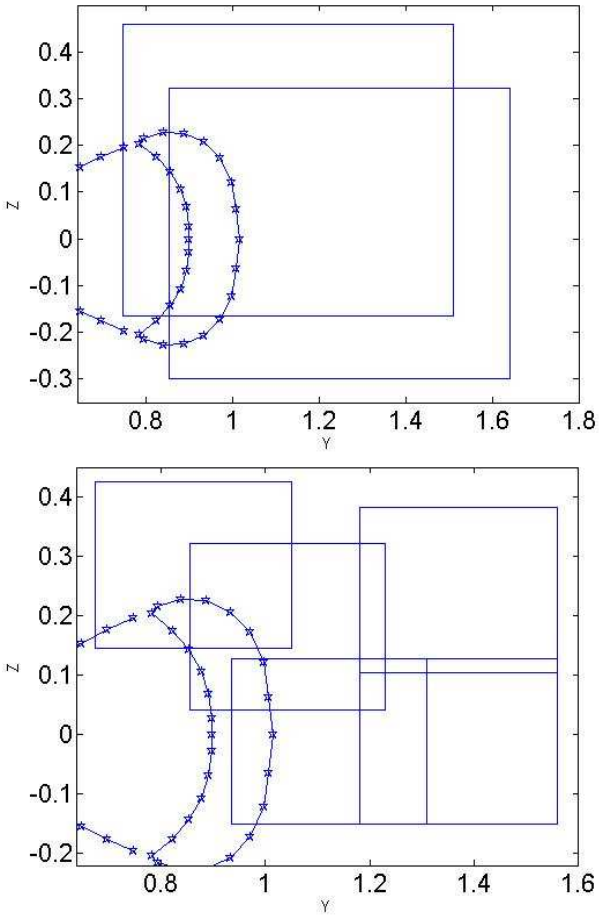

Figure 4. PIV measurement planes for the first campaign (top) and the second one (bottom).

2. Second measurement campaign

In this campaign, the camera used has a 15 Hz frequency with a 20 mm camera focal lens length. The size of the field is 387.91 x 290.843 mm^2 or 1600 x 1200 $pixels^2$. The laser is placed above the catch of the net model and the camera is outside. We measured the velocity in several plane from the net model (shown in Figure 4). The time between two images is always 0.067s and we have taken 408 instantaneous images for each measurement plane. In this case, the distance between tow points of mesh is 5.5 mm on the Oy axis and 5.5 mm on the Oz axis.

3. Third measurement campaign

This third PIV test is carried around a bottom trawl in order to characterize the flow along the horizontal parts of the trawl and to determine the evolution of the thickness of the boundary layer. In this test, the bottom trawl is placed at the bottom of the flume tank. The laser is placed above the bottom trawl and the camera is outside. The velocity fields in several planes along the bottom trawl are measured. For each plane we recorded 272 images. The time between two images is 0.067 s. The fact that the bottom trawls is in motion in the volume of water during trials entails the non validation of some PIV images: the part of the trawl illuminated by the laser is not the same for two successive images and thus, the measurements can not be validated.

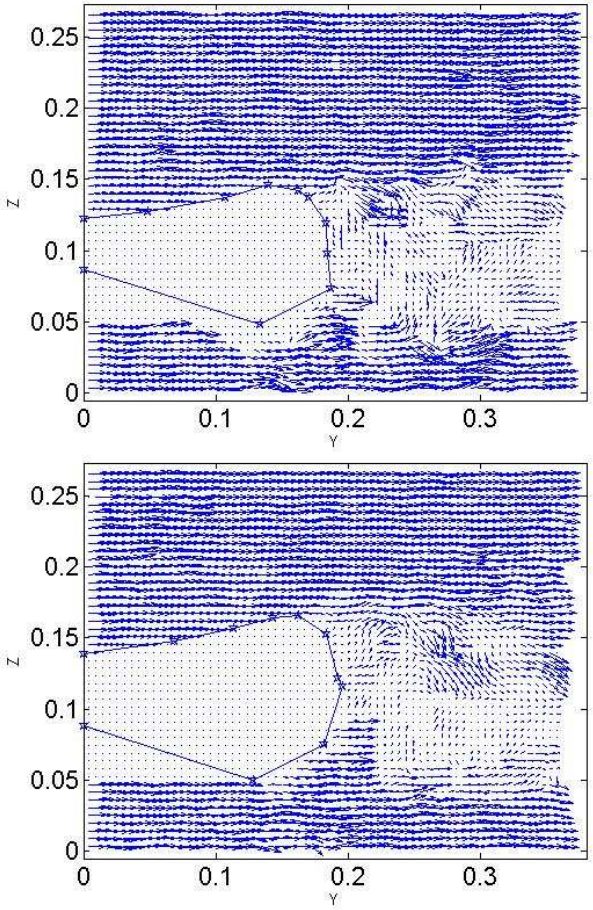

Figure 5. Instantaneous fields around the bottom trawl cod end.

For instance, the motion of the catch is oscillatory in the laser plane like shown Figure 5. Form this figure we observe different forms of the cod end in the laser plane and different locations. If it is not possible to exploit the data for means or statistics analysis, these velocity fields are interesting in term of comparison with the results obtained from the rigid cod-end. The areas where the flow is turbulent present good similarities in both kind of campaign. These measures also tell us about the possibility to improve the conditions of testing. The restriction of the movement of the trawl is necessary to make PIV measurements

exploitable. To this aim, some tests with a lower turbulent intensity of the incoming flow will be tempted. From these new measurements the characterization of the evolution of the boundary layer along the trawl should be done.

III. PROPER ORTHOGONAL DECOMPOSITION

In this section the POD theory is discussed briefly and some key features of the implementation to the PIV data are presented.

A. Mathematical concept

The application of Proper Orthogonal Decomposition to turbulent flow analysis was first proposed in 1967 by Lumley [3] as an objective method to identify deterministic features in turbulent flows. According to Lumley [3], an organized flow structure called coherent structure is the structure that has the largest mean square projection of the velocity field. This maximization leads to a Fredholm integral eigenvalue problem (Holmes et al. [4])

$$\int R(X,X')\phi(X') = \lambda\phi(X), \quad (1)$$

where X indicates the space variable and R(X,X') refers to the time averaged two point spatial correlation tensor of the velocity field. In this equation, ϕ denotes the spatial orthogonal eigenfunctions and λ is the corresponding eigenvalue. Such equation provides a finite discrete number of POD eigenfunctions, $\phi^{(n)}$ with n varying from 1 to N_{mod} which is the total number of POD modes corresponding to the dimension of the spatial correlation matrix.

Based on this flow decomposition each instantaneous fluctuating velocity field (for instance the u velocity component) can then be expressed as follows:

$$u(X,t) = \sum_{n=1}^{N_{mod}} a^n(t)\phi^n(X), \qquad (2)$$

where $a^{(n)}(t)$ is the n^{th} random temporal coefficient of projection of u(x,t) onto the n^{th} POD eigenfunction $\phi^{(n)}(X)$ and N_{mod} is the total number of the POD decomposition.

Such previous development describes the classical formulation of the POD procedure. In this description, the dimension of the spatial correlation deduced from two-dimensional PIV images is 4 $n_x \times n_y$, with $n_x \times n_y$ corresponding to the number of PIV grid points available on each flow image. Due to the possible high dimension of this kernel, an equivalent POD application has been performed by [5]. This method called snapshot POD proposes to reduce the size of the POD eigenfunction problem in computing the eigenfunctions of the spatial average temporal correlation tensor:

$$R_{nm} = (1/\mathrm{M})\left\langle u^n, u^m \right\rangle, n,m = 1,..,M \qquad (3)$$

where $M = n_x \times n_y$ is the total number of PIV snapshots. And $< >$ indicates the spatial average. The spatial eigenfunction $\phi^{(n)}(X)$ is then computed by projected each instantaneous velocity field on the $a^{(n)}(t)$ modes of the temporal correlation tensor. Finally such snapshot flow decomposition provides a similar expression of each velocity component like the one given in equation 3.

Note that both classic and snapshot flow decomposition provides orthonormal POD temporal coefficients: $a^{(n)}a^{(p)} = \delta_{np}$ with δ the Kronecker symbol and uncorrelated POD eigenfunctions satisfying $\phi^{(n)}\phi^{(p)} = \lambda^{(n)}\delta_{np}$.

Also recall that POD methodology degenerates into Fourier modes when statistically homogeneous turbulent flow is under consideration.

During the last two decades POD has become more and more a universal mathematical tool for turbulent flow analysis. Indeed, numerous POD applications have been shown its effectiveness in extracting energetic coherent structure and also in allowing the development of low order dynamical system.

B. POD implementation from PIV data

POD is performed from each PIV database described above. The purpose of such application is to examine the turbulent flow field around the rigid cod-end and the bottom trawl and especially the extraction of the large scale organized motion. Briefly for a particular test case, PIV provides a time sequence of N_t two-dimensional instantaneous velocity fields available on a $n_x n_y$ PIV grid points. Based on this available database, the first step consists in applying the Reynolds decomposition allowing to extract the time averaged mean flow field and its corresponding fluctuating part.

The second step consists in performing POD from the available instantaneous fluctuating part of the velocity field. The 2D fluctuating velocity field $V(t_k,X_{ij})$ (with (k,i,j) varying from 1 to N_t; from 1 to n_x and from 1 to n_y respectively) can be represented with a matrix of size: (N_t,$n_x \times n_y$). Using the vectorial snapshot formulation of POD procedure, the velocity correlation matrix is computed using equation 3. Then a discrete series of POD coefficient solution is obtained via the resolution of the Fredholm equation (equation 1) associated with the temporal correlation. Such resolution leads to obtain N_t POD eigenfunctions. Finally each instantaneous PIV velocity field is projected onto each POD temporal coefficient. Details on POD application from PIV database can be found in [6]. Then by projecting instantaneous velocity field onto the first POD modes, coherent structure event can then be isolated.

Globally, each instantaneous PIV velocity field is decomposed as follows: the mean flow part deduced from the classical Reynolds decomposition, the coherent part of the flow field deduced from the projection of the fluctuating velocity field onto some selected first POD modes and the residual part associated with background turbulent fluctuations.

IV. RESULTS

This section is devoted to the analysis of the turbulent flow field around a rigid cod end. First, global mean flow analyses are performed. Then Proper Orthogonal Decomposition is implemented to highlight the large scale structures of the flow around the model. Finally, based on the extraction of these flow structures, spectral analysis is performed leading to the analysis of the vortex shedding frequency. Based on such analyses, we expect to enhance the knowledge of the spatial flow structure of wake and its associated frequency.

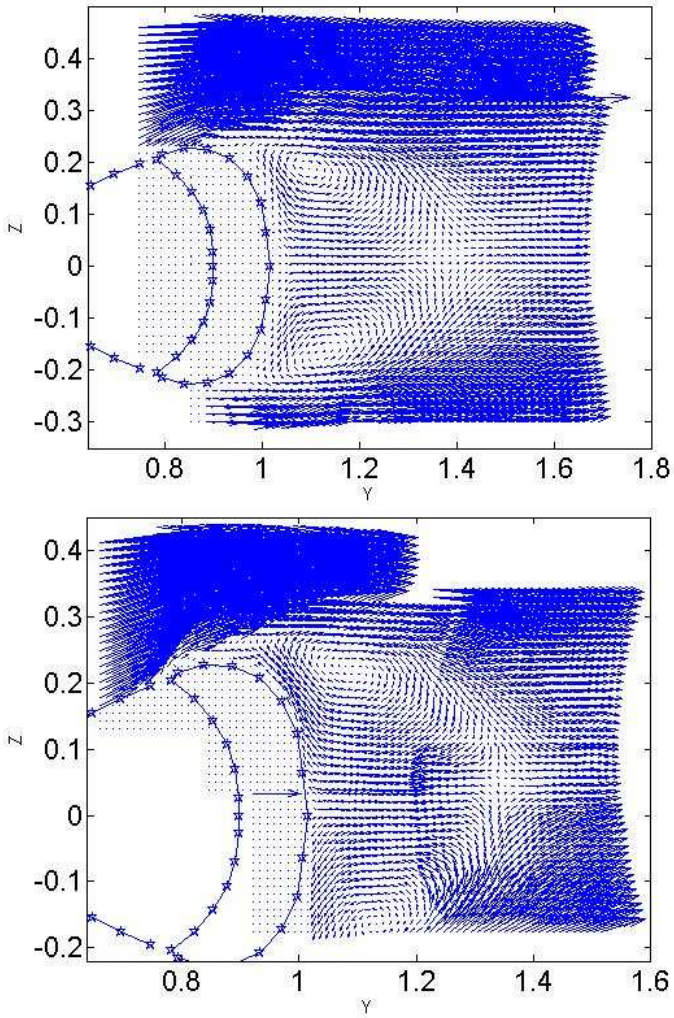

Figure 6. Mean velocity field. Top: computed in each PIV plane of the first measurement campaign. Bottom: computed in each PIV plane of the second measurement campaign.

A. *Mean analysis of the flow field*

Based on the first measurement campaign (section II-B-1), the temporal mean flow field is computed from the 380 instantaneous velocity fields in each measurement plane. In a similar manner, using the second measurement campaign (section II-B-2), the mean flow field is computed in each available PIV plane from the knowledge of 408 instantaneous velocity fields. Figure 6 displays the resulted mean flow field for each PIV campaign. On this figure, the vertical patterns of the wake are clearly visible. Indeed, the near wake of the porous structure is dominated by two large counter rotating vortices which are symmetric along the z=0 axis.

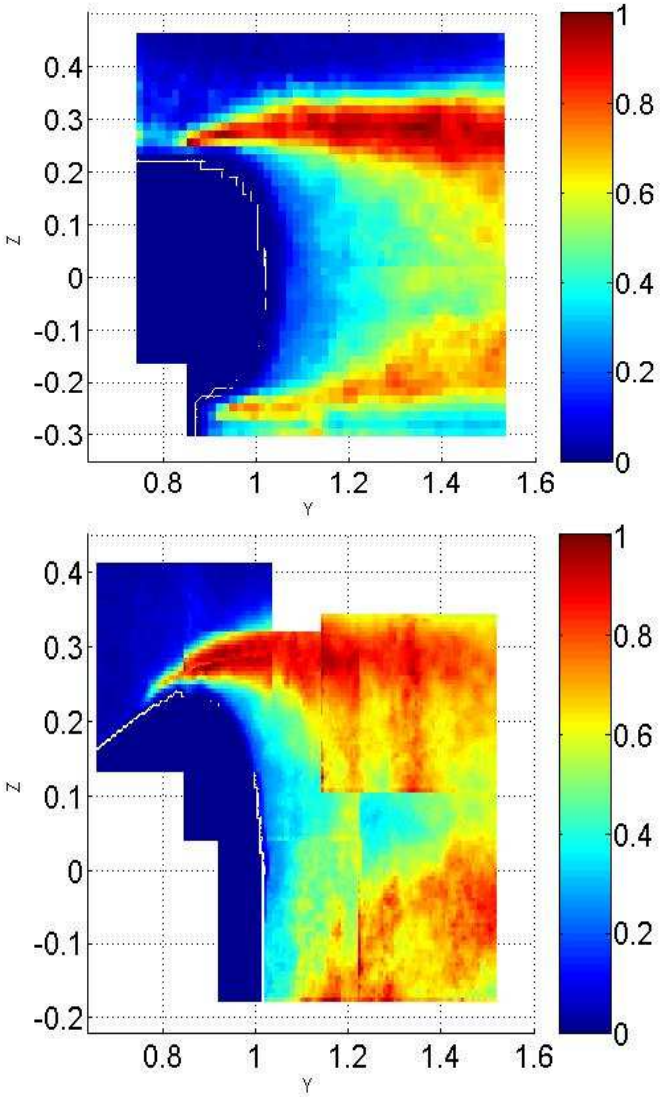

Figure 7. Normalized turbulent kinetic energy: Top: computed in each PIV plane of the first measurement campaign. Bottom: computed in each PIV plane of the second measurement campaign.

To access the turbulence levels of the flow, the mean turbulent kinetic energy is computed from each PIV plane investigated in the first two measurement campaigns. Figure 7 shows this quantity for both PIV measurements. As it has been observed in Figure 6, the turbulent wake is clearly identified. Indeed, the separated shear layer is observed in this figure. Note that some differences are observed between both graphs presented on Figure 7 and especially for distances far from y=1.4 m. Indeed, the levels of normalized kinetic energy levels deduced from the second measurements are quite superior to the ones computed from the first PIV

database. This is directly related to the spatial resolution of the PIV meshgrid which is different in both measurements. Due to the high spatial resolution used in the second database, the measurements allow to access to smaller scale structures which may be more turbulent than the structures able to be measured from the first database.

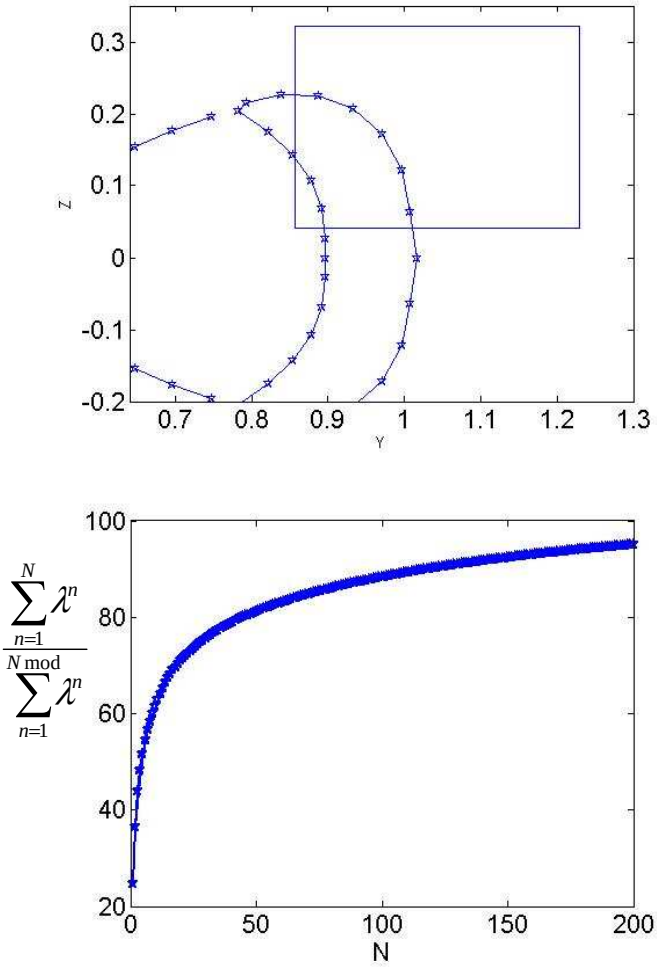

Figure 8. Top: Detailed PIV measurement plane under POD investigation. Bottom: the POD energy convergence.

B. POD analysis

Based on the first and second measurement campaigns, POD is implemented to extract the energetic large scale coherent structures present in each plane. In this paper, we only present selected POD analysis performed in measurement planes located in the wake of the structure. More precisely, we focus on the PIV measurement plane located in the upper right corner of the porous structure. Based on 408 instantaneous velocity fields available in this plane, snapshot POD is performed leading to obtain Nt=408 POD eigenfunctions. Figure 8 represents the POD energy convergence that is the percentage of the energy contained in each POD mode.

Note on this figure the x-axis is limited to 200 in order to better appreciate the energetic content of the first POD modes. Then the first mode and the first 44 ones contains respectively 25 % and 80 % of the total kinetic energy. An illustration of the potential of this methodology is given on Figure 9. On this figure, a raw instantaneous velocity vector field is given and its projection onto the 44 POD modes corresponding to 80% of the total energy is also provided. Note that quasi similar results are obtained for each instantaneous velocity field projected onto these first POD modes. On this figure, it is clearly demonstrated that POD procedure extract the coherent structure embedded in the background turbulent flow.

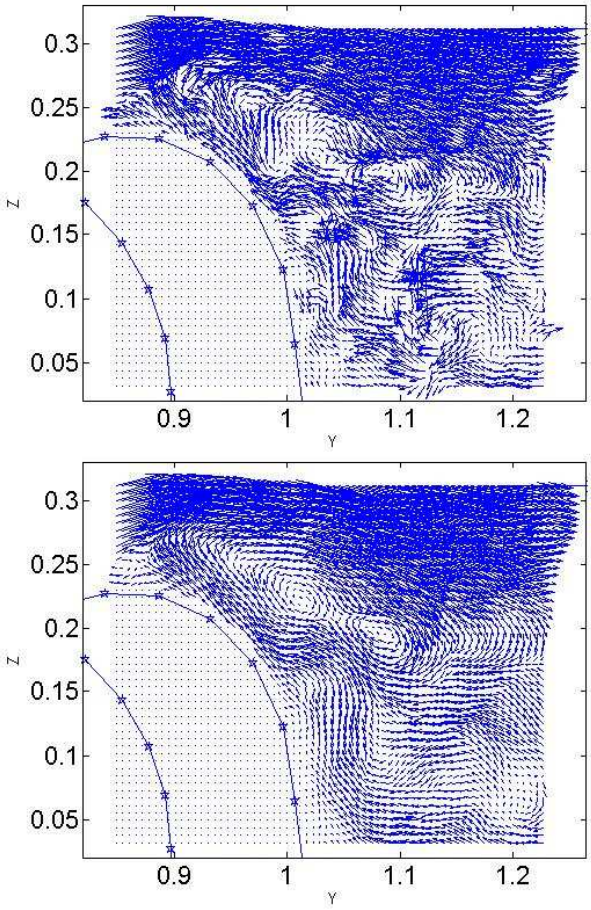

Figure 9. Top: Instantaneous PIV velocity field . Bottom same instantaneous PIV velocity field projected on the first 44 pod modes.

Based on this flow representation, it is then possible to analyze the large scale flow dynamic in the wake of the porous structure. Then each instantaneous velocity field measured in this plane is projected onto the same number of POD modes. An illustration of the resulted projected instantaneous velocity field is displayed on Figure 10. This last figure presents 6 successive instantaneous velocity fields. This ‘dynamical’ representation permits to observe the pairing process occurring in the vortex shedding wake. Indeed, two coherent structures merge themselves to form another coherent flow structure. Otherwise, on each of these figures, a surface color has been added in order to mark the

presence of the vortex structure. This marker is based on the usual Q criterion used to characterize the flow structures present en turbulent flows. Briefly, this local criterion initially proposed by Hunt et al. [7] is based on the analysis of invariants of the velocity gradient tensor. The criterion is then defined as follows:

$$Q = \frac{1}{2}(\|\Omega\|^2 - \|S\|^2), \quad (4)$$

where S and Ω are the symmetric and antisymmetric parts of the velocity gradient, and ||.|| indicates the norm. A vortex is then defined with Q>0.

Applying this criterion to instantaneous PIV velocity field may be corrupted due to the presence of background turbulent fluctuations and also eventually measurement errors. We then propose to compute this criterion using instantaneous velocity field projected onto the first POD modes. Indeed, POD procedure acts as a filtering technique for the PIV instantaneous velocity fields.

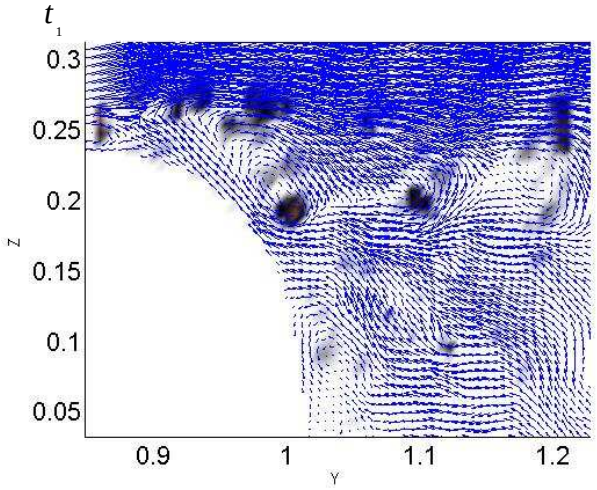

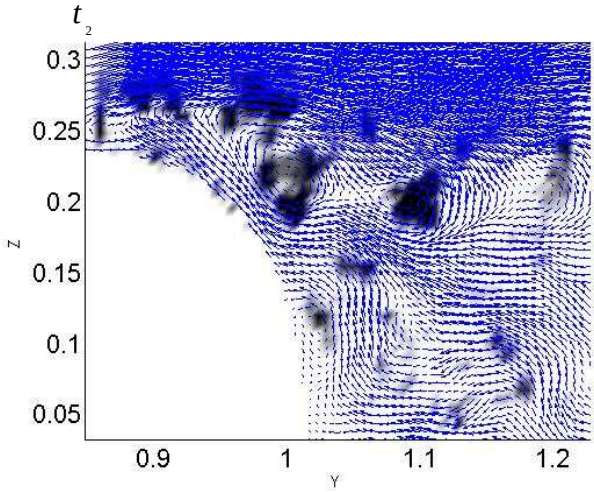

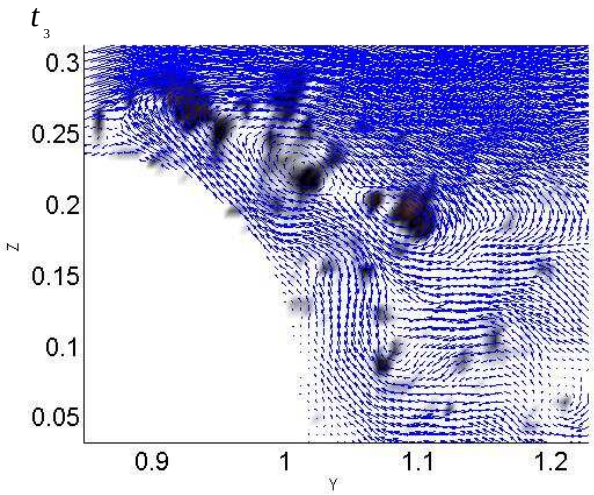

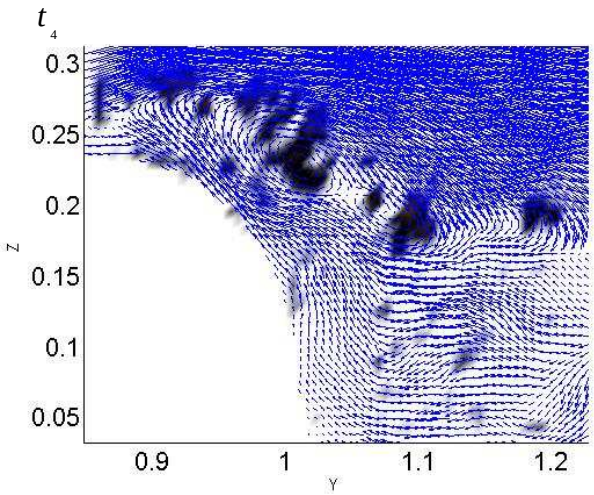

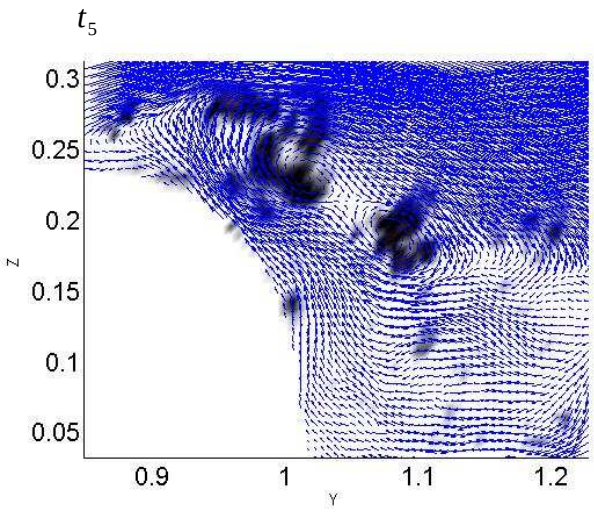

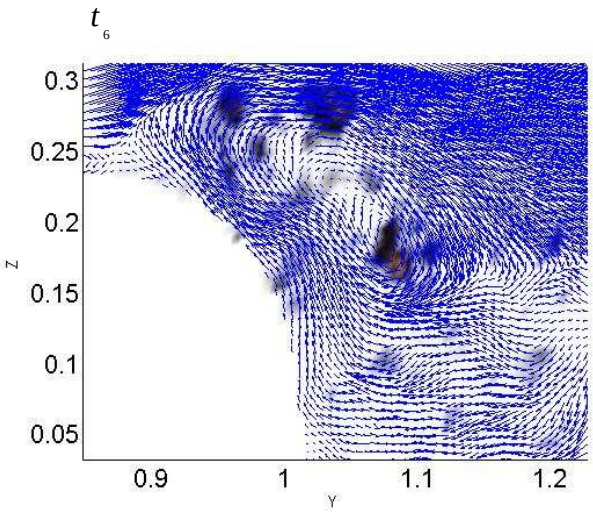

Figure 10. Successive time instantaneous vector fields projected on the first 44 pod modes which contain 80% of the total kinetic energy. Isosurfaces of Q criterion is superimposed onto each velocity vector field. Black color indicates the high positive level of Q.

C. Spectral analysis

Due to the high frequency resolution of the second PIV database, a frequency analysis of the vortex shedding frequency can be performed. Such analysis associated with a porous structure has not yet been fully investigated. The particularity of trawl or related fishing nets concerns the difficulty in properly numerically modeling these porous structures. Nowadays such investigation can then be performed essentially from experimental measurements. Then one of the purpose of the current vortex shedding frequency analysis consists in trying to compare and to link our results to previous existing ones obtained from 'classical' turbulent wake flow behind a cylinder or a sphere for instance.

In the past, transitional and fully turbulent wake flows of two and three-dimensional bluff-body geometries have been intensively studied by many researchers for many decades. It is still one of the most active research fields in fluid mechanics due to numerous potential engineering applications. Then a lot of previous studies have been devoted to the analyses and the control of the wake behind a cylinder or a sphere. Thus, based on numerous experimental and numerical investigations [8] it has been observed that the wake transition differs greatly for the cylinder and the sphere respectively.

Such analysis is great dependent of the geometry of the body, knowing that current porous structure has a quite complex geometry. Furthermore, previous vortex shedding frequency analyses have shown that they are Reynolds number-dependent. The Strouhal number defined as follows: $f = U_{ref} / d$ is based on the reference streamwise velocity U_{ref} = 0.57 m/s, the length $d = 0.454$ *m* corresponding to the diameter of the trawl (see figure 11). In this paper, we present selected power spectra of the streamwise velocity component computed at three different locations. These locations are given on Figure 11. The first point (p1) is located upstream the catch while the second point (p2) is in the beginning of the near field wake of the flow. The third point (p3) is in the wake of the porous structure. Note that this last point begins to a different PIV plane measurement than the other ones.

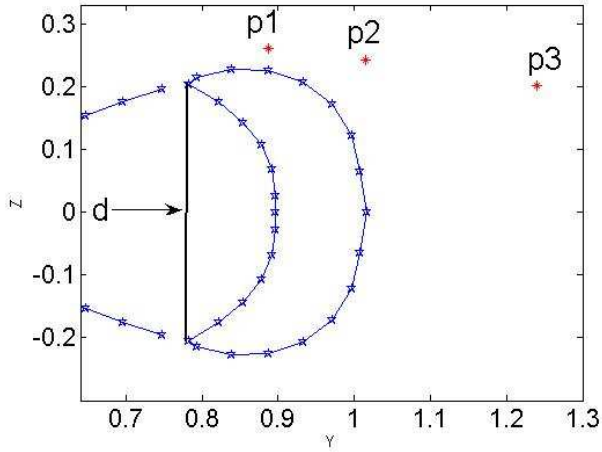

Figure 11. Detailed of the locations from which instantaneous velocity is used to compute its corresponding power spectrum. The length d is used as reference length to compute the Strouhal number.

As a first step, the power spectra are directly computed from the raw available PIV database. Figure 12 presents both power spectra of the u velocity component measuring at point p1 and p2 respectively. On such figure, the maxima peaks associated with p1 and p2 measurements correspond respectively to a Strouhal number of 0.27 and 0.32. These values are directly related to the flow instabilities of the boundary layer and the shear layer. Conversely, the power spectrum computed in the wake shows a typical frequency corresponding to a Strouhal number of 0.185 (see figure 13-a). This is associated with the Kelvin-Helmhotz instability in the detached shear layers. This Strouhal number is similar to the one obtained in the wake of flow behind a cylinder or and sphere.

As a second step, POD procedure is applied to PIV database and power spectra are now computed from the velocity component u projected onto selected POD modes. Figures 13-b, 13-c and 13-d display the power spectrum associated with the velocity u component projected:

- onto the first 5 POD modes,
- onto the POD modes varying from 6 to 20
- onto the POD modes from 21 to $N_{mod}=N_t=408$.

Note that in this measurement plane, the first 5 POD modes contains 53% of the total kinetic energy and the first 20 modes contains more than 70% of the total kinetic energy. Figure 13-b clearly identified the first frequency peak observed on figure 13-a deduced from raw available PIV database. Thus, the first POD modes can be associated to the main flow instability. Conversely, when regarding figure 13-

c, it is observed that the flow field projected onto the POD modes from 6 to 20 is associated with the first subharmonic (St~=0.36). Finally the residual flow field projected onto the residual pod mode corresponds to background turbulent fluctuations without any selected frequency.

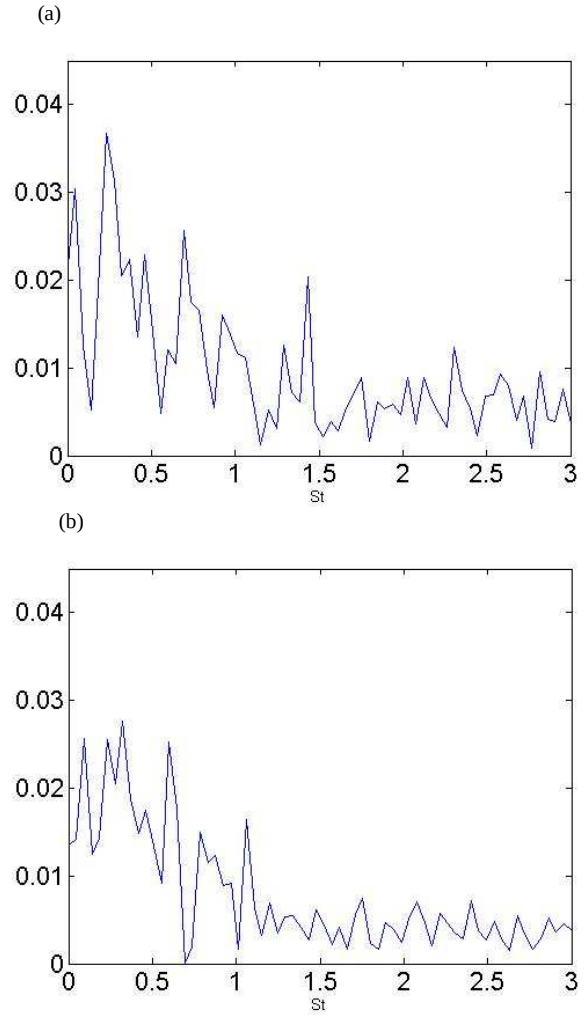

Figure 12. Spectra of the longitudinal velocity expressed as a function of Stourhal number. Top: Computed in point p1. Bottom: Computed in point p2.

V. CONCLUSION

The control of boundary layers or more generally the hydrodynamics instabilities of the near wake past the porous structure in high Reynolds number flows, is still a matter of central interest in our HydroPêche project devoted to the reduction of drag of the gear. Indeed, the motivation of current study is to achieve drag reduction but also to provide additional information about the turbulent flow characteristics of the flow around the trawl.

In this experimental analysis, the main characteristics of the flow around a trawl have been examined. The global characterization of the flow including the spatial representation of the mean flow field and the mean kinetic energy may be quite interesting for the numerical computation of the drag coefficient of such a porous structure.

The implementation of the POD procedure has been proved its effectiveness in showing the main flow organization of such a turbulent flow. Finally, the POD application allows the extraction of the instantaneous flow structures making possible to dynamically follow these structures and to estimate their dynamical space and time evolution.

Furthermore a spectral analysis allows the investigation of the vortex shedding frequency of this flow. We then observe that the turbulent wake flow of this fixed porous structure can be related to previous analyses of a turbulent wake flow behind a sphere and/or a cylinder.

Finally, even if these results give some great new information about the turbulent flow, an extension of this study has to be perform from the turbulent flow around a moving fishing net. The third PIV campaign is under investigation and similar analyses will be performed and presented during the E-fishing congress.

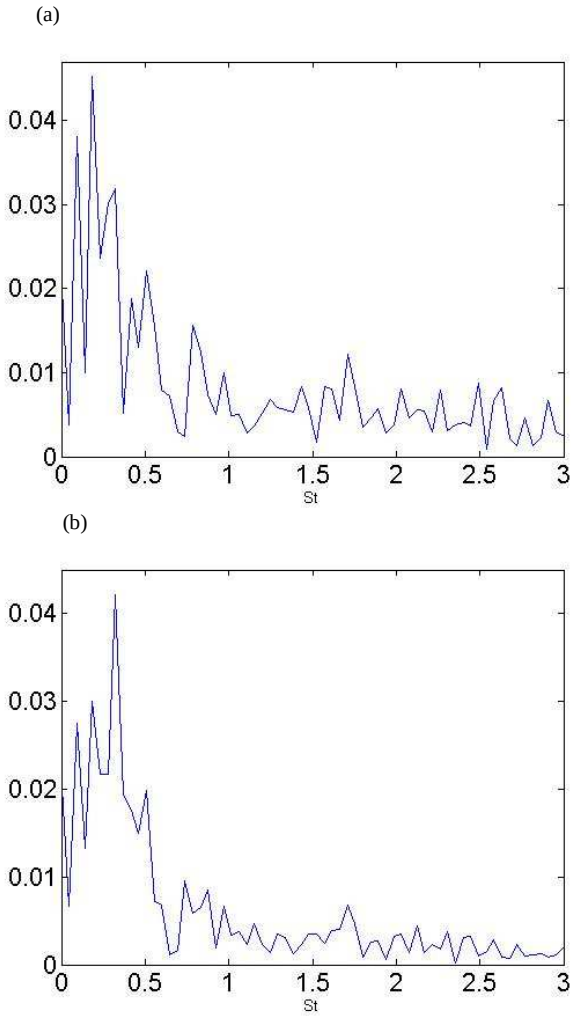

(c)

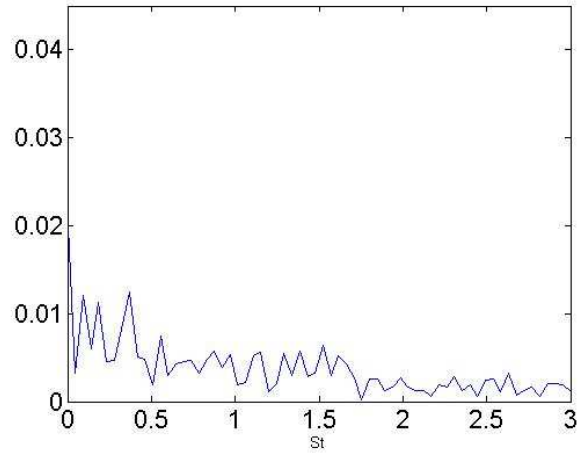

(d)

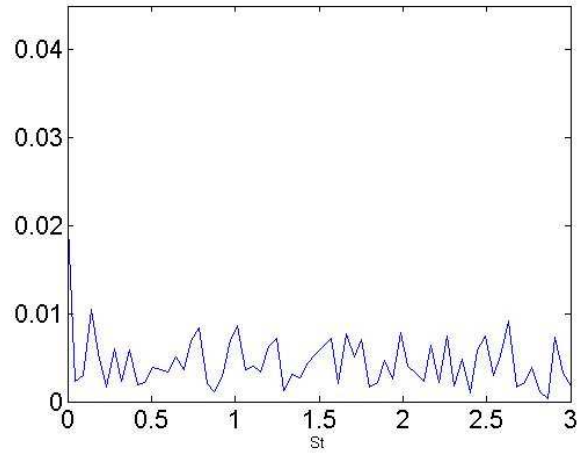

Figure 13. Power spectra computed from the u velocity component saved at p3 location and projected onto (a) the whole set of available POD modes (raw original PIV database) ; (b) the first 5 POD modes; (c) from POD mode number 6 to POD mode number 20 ; (d) the residual POD modes (up to mode number 21.

REFERENCES

[1] G. Germain. HydroPêche: "a way to improve energy efficiency of fishing devices," E-Fishing 2010 unpublished.

[2] G. Pichot, G. Germain, D. Priour, "On the experimental study of the flow around a fishing net," Journal of Mechanics B/Fluids, Vol. 28, pp. 103-116, 2008.

[3] J.L.Lumley. "The structure of inhomogeneous turbulent flows. Atmospheric Turbulence and Radio Wave Propogation," Vol. In A.M.Yaglom and Tararsky, pp. 166-178, 1967.

[4] P. Holmes, J.L. Lumley and G. Berkooz,. "Turbulence, Coherent Structures, Dynamical Systems and Symmetry," Cambridge Monographs on Mechanics, Cambridge, 1996.

[5] H.Sirovich. "Turbulence and the dynamics of coherent structures, part i : Coherent structures," Quart. Appl.Mech. Vol. 45-3, pp. 561-590, 1987.

[6] P. Druault, P. Guibert, F. Alizon, "Use of proper orthogonal decomposition for time interpolation from PIV data," Journal Experiment in fluids, Vol. 39 , pp. 1009-1023, 2005.

[7] Hunt J.C.R, Waray ,CCA, Moin P, "Streams and, Convergence zones in turbulent flows, " center for turblence Research report CTR-S88, Stanford University, pp. 193-207, 1988.

[8] C H K Williamson "Vortex dynamics in the cylinder wake," Review of Fluid Mechanics, Vol. 28, pp. 477-539, 1996.